AD-A088 365 SRI INTERNATIONAL MENLO PARK CA F/G 4/1
MAGNETIC-FIELD-ALIGNED CHARACTERISTICS OF PLASMA BUBBLES IN THE--ETC(U)
JUL 79 R T TSUNODA DNA001-79-C-0153
UNCLASSIFIED DNA-5150T NL

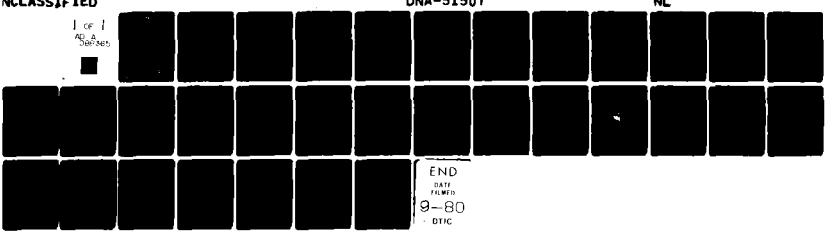

(12) LEVEL II

DNA 5150T

MAGNETIC-FIELD-ALIGNED CHARACTERISTICS OF PLASMA BUBBLES IN THE NIGHTTIME EQUATORIAL IONOSPHERE

Roland T. Tsunoda
SRI International
333 Ravenswood Avenue
Menlo Park, California 94025

1 July 1979

Topical Report 3 for Period 2 April 1979—1 July 1979

CONTRACT No. DNA 001-79-C-0153

APPROVED FOR PUBLIC RELEASE;
DISTRIBUTION UNLIMITED.

THIS WORK SPONSORED BY THE DEFENSE NUCLEAR AGENCY
UNDER RDT&E RMSS CODE B322079462 I25AAXHX64009 H2590D.

Prepared for
Director
DEFENSE NUCLEAR AGENCY
Washington, D. C. 20305

Destroy this report when it is no longer needed. Do not return to sender.

PLEASE NOTIFY THE DEFENSE NUCLEAR AGENCY, ATTN: TISI, WASHINGTON, D.C. 20305, IF YOUR ADDRESS IS INCORRECT, IF YOU WISH TO BE DELETED FROM THE DISTRIBUTION LIST, OR IF THE ADDRESSEE IS NO LONGER EMPLOYED BY YOUR ORGANIZATION.

UNCLASSIFIED

SECURITY CLASSIFICATION OF THIS PAGE (When Data Entered)

REPORT DOCUMENTATION PAGE	READ INSTRUCTIONS BEFORE COMPLETING FORM
1. REPORT NUMBER: DNA 5150T — HI-E300 879	2. GOVT ACCESSION NO.: AD-A088 365
3. RECIPIENT'S CATALOG NUMBER: NO.	
4. TITLE (and Subtitle): MAGNETIC-FIELD-ALIGNED CHARACTERISTICS OF PLASMA BUBBLES IN THE NIGHTTIME EQUATORIAL IONOSPHERE	5. TYPE OF REPORT & PERIOD COVERED: Topical Report, 3 for Period 2 Apr [illegible]—1 Jul 1979
6. PERFORMING ORG. REPORT NUMBER: SRI Project 8164	
7. AUTHOR(s): Roland T. Tsunoda	8. CONTRACT OR GRANT NUMBER(s): DNA 001-79-C-0153
9. PERFORMING ORGANIZATION NAME AND ADDRESS: SRI International, 333 Ravenswood Avenue, Menlo Park, California 94025	10. PROGRAM ELEMENT, PROJECT, TASK AREA & WORK UNIT NUMBERS: Subtask I25AAXHX640-09
11. CONTROLLING OFFICE NAME AND ADDRESS: Director, Defense Nuclear Agency, Washington, D.C. 20305	12. REPORT DATE: 1 Jul 1979
	13. NUMBER OF PAGES: 32
14. MONITORING AGENCY NAME & ADDRESS (if different from Controlling Office)	15. SECURITY CLASS (of this report): UNCLASSIFIED
	15a. DECLASSIFICATION/DOWNGRADING SCHEDULE

16. DISTRIBUTION STATEMENT (of this Report)

Approved for public release; distribution unlimited.

17. DISTRIBUTION STATEMENT (of the abstract entered in Block 20, if different from Report)

18. SUPPLEMENTARY NOTES

This work sponsored by the Defense Nuclear Agency under RDT&E RMSS Code B322079462 I25AAXHX64009 H2590D.

19. KEY WORDS (Continue on reverse side if necessary and identify by block number)

Equatorial Spread F
Plasma Bubbles
Ionospheric Irregularities
Incoherent Scatter

20. ABSTRACT (Continue on reverse side if necessary and identify by block number)

During the past three years, the Defense Nuclear Agency (DNA) has conducted a series of rocket experiments from the Kwajalein Atoll, Marshall Islands, to investigate the character of intense, scintillation-producing irregularities that occur in the nighttime equatorial ionosphere. Because the source mechanism of equatorial irregularities, believed to be the Rayleigh-Taylor instability, is analogous to that which generates plasma-density striations in a nuclear-induced environment, there is considerable interest in the underlying

DD FORM 1 JAN 73 1473 EDITION OF 1 NOV 65 IS OBSOLETE

UNCLASSIFIED

SECURITY CLASSIFICATION OF THIS PAGE (When Data Entered)

20. ABSTRACT (Continued)

physics that controls the characteristics of these irregularities. A primary objective of ALTAIR investigations of equatorial irregularities is to seek an understanding of the underlying physics by establishing the relationship between meter-scale irregularities (detected by ALTAIR), and large-scale plasma depletions (or "bubbles") that contain the kilometer-scale, scintillation-producing irregularities. An important application of this relationship has been the use of ALTAIR as a real-time locator of intense irregularities for the purpose of rocket launch criteria.

Measurements of both incoherent-scatter (IS) and backscatter from field-alined irregularities (FAI) were made in 1978 with ALTAIR, a fully-steerable high-power radar, to investigate the magnetic-field-aligned characteristics of equatorial plasma bubbles. By operating the radar in a latitude-scan IS mode, we were able to map the location and percentage depletion of plasma bubbles as a function of altitude and latitude. And, by showing that backscatter from FAI is spatially collocated with the upper wall of plasma bubbles, were able to use the spatial displacement of a field aligned backscatter region to estimate the upward bubble velocity. Besides showing that plasma bubbles are indeed aligned along magnetic field lines, we use this data set to show that a plasma bubble with a percentage depletion of as much as 90% does not have as large an upward velocity as predicted by two-dimensional models. Instead, the inferred bubble velocity is shown to be in better agreement with the bubble velocity predicted by theoretical models using flux-tube-integrated value of electron density and Pedersen conductivity. The need to use flux-tube-integrated values when comparing theory and observation is further stressed by the presence of a nonuniform latitudinal distribution of electron density (i.e., the equatorial anomaly) that was found in the latitude-scan data.

CONTENTS

ILLUSTRATIONS

I INTRODUCTION

The fundamental process that initiates the formation of equatorial irregularities appears to be the Rayleigh-Taylor instability [Dungey, 1956; Balsley et al., 1972; Haerendel, 1974; Hudson and Kennel, 1975]. This theory [Scannapieco and Ossakow, 1976; Ossakow and Chaturvedi, 1978] predicts that plasma-depleted regions, or "bubbles", with scale sizes greater than a few tens of kilometers (transverse to the geomagnetic field) are formed in the bottomside of the F layer. These bubbles then buoyantly rise upward into the topside of the F layer. This theoretical model is strongly supported by qualitative features that have been observed in the nighttime equatorial ionosphere by in-situ measurements [Hanson and Sanatani, 1973; Kelley et al., 1976; McClure et al., 1977; Morse et al., 1977] and by incoherent-scatter (IS) radar [Towle, 1979; Tsunoda, 1979]. These measurements have shown that the observed bubbles have characteristics that imply their origin at lower altitudes and subsequent upward movement.

Further evaluation of this theory, however, requires a more quantitative comparison between theoretical model and experimental result. Experimental data are needed to test the basic assumptions implicit in the theoretical models as well as to verify the theoretically predicted characteristics. For example, a basic assumption is that the geomagnetic field lines can be treated as electric equipotentials. This assumption, and the need to keep theoretical analysis tractable, have led to the treatment of the Rayleigh-Taylor instability in two dimensions with the use of local values of both electron density and ion-neutral collision frequency. Haerendel [1974], however, has pointed out [see also Balsley et al., 1972] that the important parameters are the magnetic flux-tube-integrated values of electron density and Pedersen conductivity. Haerendel [1974] and Anderson and Haerendel [1979] have shown that the use of flux-tube-integrated values (instead of local values) lead to

significant differences in the predicted instability growth characteristics and plasma bubble dynamics.

Besides consideration of the use of flux-tube-integrated quantities when comparing theory and experiment, it will be noted that there is a paucity of experimental evidence showing that plasma bubbles involve entire magnetic flux tubes. The best evidence published to date is that of Dyson and Benson [1978]. Using topside ionograms taken from Alouette II and ISIS I satellites, they inferred the existence of depleted magnetic flux tubes in the equatorial ionosphere by interpreting anomalous ionogram traces in terms of high-frequency radio-wave propagation in plasma bubbles.

Other experimental evidence, indicating the field-aligned nature of plasma bubbles, includes rocket measurements by Morse et al. [1977] and airborne 6300A airglow measurements by Weber et al. [1978]. Morse et al. [1977] found that electron-density structural features were correlated over several hundred kilometers in latitude, where the separation distance was determined by the upleg and downleg of the rocket trajectory. Weber et al. [1978] showed that 6300A airglow depletions were magnetic north-south aligned, and extended more than 1200 km in that direction. They further showed through comparisons with ionosonde data, that the airglow depletions resulted from local elevations in the bottomside F layer. They proposed that these airglow depletions might be bottomside F-layer signatures of plasma bubbles.

In this report, we present direct evidence from IS measurements that plasma bubbles are indeed magnetic field aligned, and that they extend over many degrees of magnetic latitude. The results were obtained from a radar experiment in which ALTAIR, a fully-steerable IS radar, was operated in a latitude-scan IS mode. The electron-density profiles obtained during the latitude scan are also used to show that there is a substantial latitudinal variation in background electron density. The magnetic-field-aligned characteristics of the plasma bubble, including its upward velocity, are shown to be in good agreement with the theoretical model of Anderson and Haerendel [1979], which uses flux-tube-integrated quantities.

II EXPERIMENTAL CONSIDERATIONS

The experiment consisted of operating ALTAIR, a fully-steerable incoherent-scatter (IS) radar, in two kinds of scans: (1) an elevation (or latitude) scan in the magnetic meridian (9°E true azimuth), and (2) an east-west scan. The first scan consisted of making IS measurements at discrete elevation angles to obtain the background electron-density profile as a function of latitude. The second scan was used to map the spatial distribution of equatorial field-aligned irregularities (FAI)--in particular, the backscatter plumes first reported by Woodman and La Hoz [1976]. The mapping of plumes with ALTAIR has previously been reported by Tsunoda et al. [1979], Tsunoda and Towle [1979], Towle [1979], and Tsunoda [1979].

The location of ALTAIR and the east-west scan geometry for mapping equatorial FAI are shown in Figure 1. ALTAIR is located in the Kwajalein Atoll, Marshall Islands, at a magnetic dip latitude of 4.3°N. The radar was operated for this experiment at 155.5 MHz, transmitting a 30-μs pulse through a 46-m paraboloid antenna having a 2.8° beamwidth. The scanned sector is shown by a shaded region, in which the radar beam becomes orthogonal to the geomagnetic field. Examples of contours showing the locations of exact magnetic orthogonality--at altitudes of 105, 400, and 700 km--are also shown in Figure 1. The latitude scan was made in the magnetic meridian, perpendicular to the east-west scan shown in Figure 1 (in the plane containing the magnetic north vector). The scan was stepped (south to north) through discrete beam positions, starting and ending at 20° elevation angle with increments of 10°. Data samples, spaced at 4.5-km range intervals, were collected and averaged for one minute (2400 samples) at each beam position, with the total scan being completed in about 15 minutes. The data samples were also averaged in range, using a five-point, weighted (12321) running average.

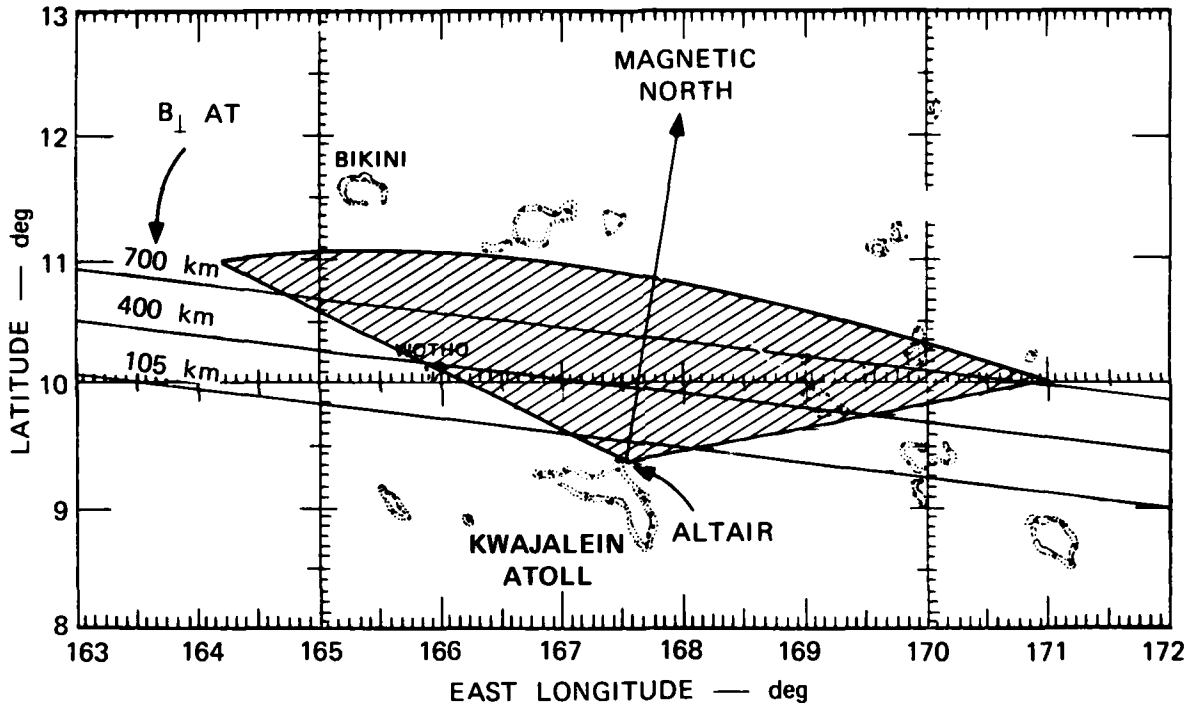

FIGURE 1 MAP SHOWING THE LOCATION OF ALTAIR AND THE RADAR SCAN GEOMETRY

The radar data were obtained on 18 August 1978, a night of high spread-F activity. We selected a data set, consisting of a latitude scan followed by an east-west scan, both taken late at night when spread-F activity was in a general decline. This choice was made because plasma-depleted regions were more easily discernible under less disturbed conditions, when the structure in electron density did not completely obscure the presence of isolated bubbles. The backscatter map obtained from the east-west scan is used to identify the backscatter plume associated with the plasma bubble of interest, and the electron density profiles obtained from the latitude scan are used to characterize the plasma bubble and the background ionosphere.

III RESULTS

The results are organized as follows: we first describe the time history of the vertical movement of the background F layer during the night when the latitude-scan data of interest were taken. This is done because knowledge of the post-sunset rise of the F layer and its subsequent downward motion is needed in later discussions of the results. After describing the vertical movement of the background ionosphere over ALTAIR, we present the latitude-scan IS data with which we characterize the magnetic-field-aligned characteristics of a plasma bubble and the background F layer. Data of backscatter from FAI are shown to be collocated with the upper wall of the plasma bubble, and then used to estimate the upward plasma-bubble velocity. This unique set of measurements allows us to evaluate the various theoretical models of plasma bubble velocity.

The altitude of the bottomside of the F layer, plotted as function of time, is shown in Figure 2. For convenience, we have arbitrarily selected the altitude at which the electron density was 10^5 el/cm^3. (By this choice of F-layer altitude characterization, there is a tendency to overestimate the vertical velocity produced by the east-west electric field. However, the other contributing factors--reduction of electron density by recombination, and steepening of the bottomside of the F layer during the electrodynamic lifting of the F layer--are small, and do not alter the results in this paper.) All of the data shown were obtained by IS measurements with the ALTAIR beam directed at high elevation angles. In other words, the plot shown in Figure 2 corresponds to the behavior of the F layer overhead of ALTAIR.

When the radar was first turned on at 0745 UT (1855 local time), the bottomside of the F layer was at a 330-km altitude. The F layer rose rapidly reaching an altitude of 440 km by 0820 UT. Using these two data points, the upward F-layer velocity was estimated to be about 50 m/s.

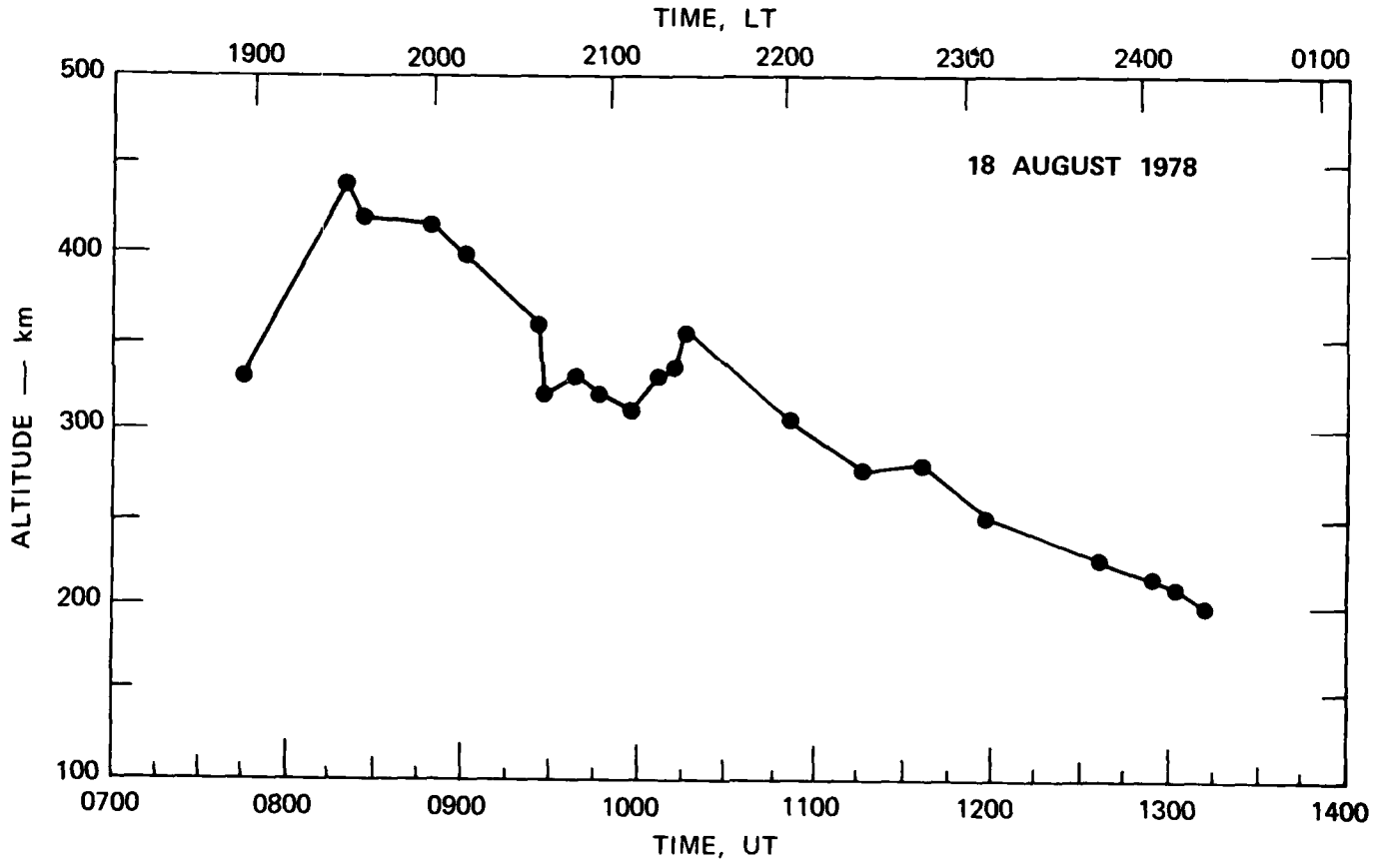

FIGURE 2 ALTITUDE OF THE BOTTOMSIDE OF THE F LAYER (where the electron density equals 10^5 el/cm^3) vs. TIME

After 0830 UT (except for the perturbation in F-layer altitude that occurred between 0930 and 1051 UT), the F layer descended at a nearly uniform speed of 13 m/s. The latitude-scan data of interest was taken between 1130 and 1200 UT, when the bottomside of the F layer and descended to 250 km.

The altitude of 440 km, attained by the bottomside of the F layer on this night, represents one of the highest altitudes ever reached by the F layer in all of the nights of ALTAIR operation in 1978. The ascent rate of the F layer also represents one of the highest vertical velocities observed. (In this section it is also shown that this post-sunset rise of the F layer was accompanied by an evening enhancement of the equatorial anomaly.) Correspondingly, plume backscatter activity on this night was also one of the most disturbed. The descent of the F layer was accompanied by a general weakening of backscatter plume activity. Plume activity had virtually ceased by 1248 UT when the bottomside of the F layer had descended to 220 km. (Tsunoda et al. [1979] presented similar examples in which plume activity was very weak when the bottomside of the F layer was less than 250 km.)

The electron density profiles obtained from the elevation scan in the magnetic meridian are shown in Figures 3 and 4. The profiles shown were taken at 10° intervals in radar elevation angle, starting at 40° (to the south) and ending at 30° (to the north). Each profile, plotted using a logarithmic scale, is centered over a tick mark labeled with the time at which the IS data were collected. The electron density for any given profile can be scaled from the abscissas as follows: for any given profile, let the tick mark directly beneath the profile be equal to 10^5 el/cm^3. All other tick marks for that profile represent decade increments in electron density. For example, the tick mark directly beneath the profile taken at 1133:40 UT corresponds to an electron density of 10^6 el/cm^3 for the profile taken at 1132:35 UT. To facilitate comparisons of the profiles, we have shaded that portion of each profile that is greater than 10^5 el/cm^3.

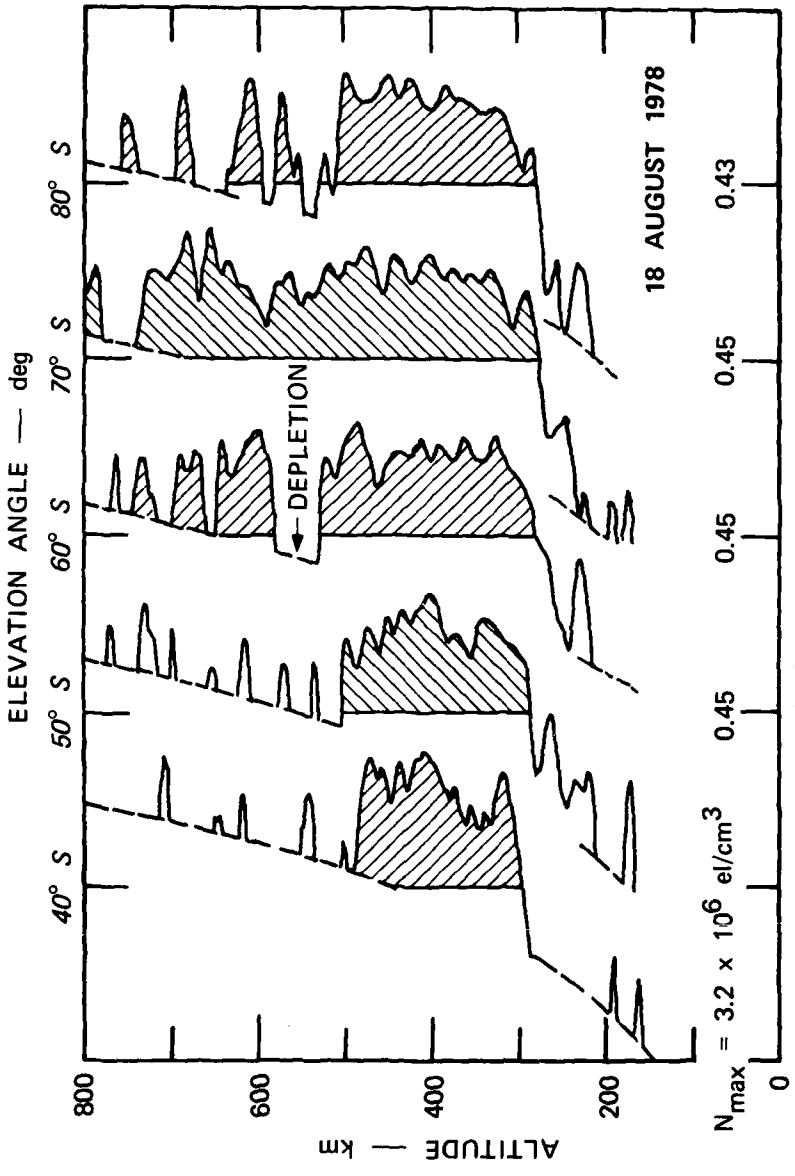

FIGURE 3 ELECTRON DENSITY PROFILES OBTAINED FROM THE SOUTH HALF OF THE ELEVATION SCAN BY ALTAIR

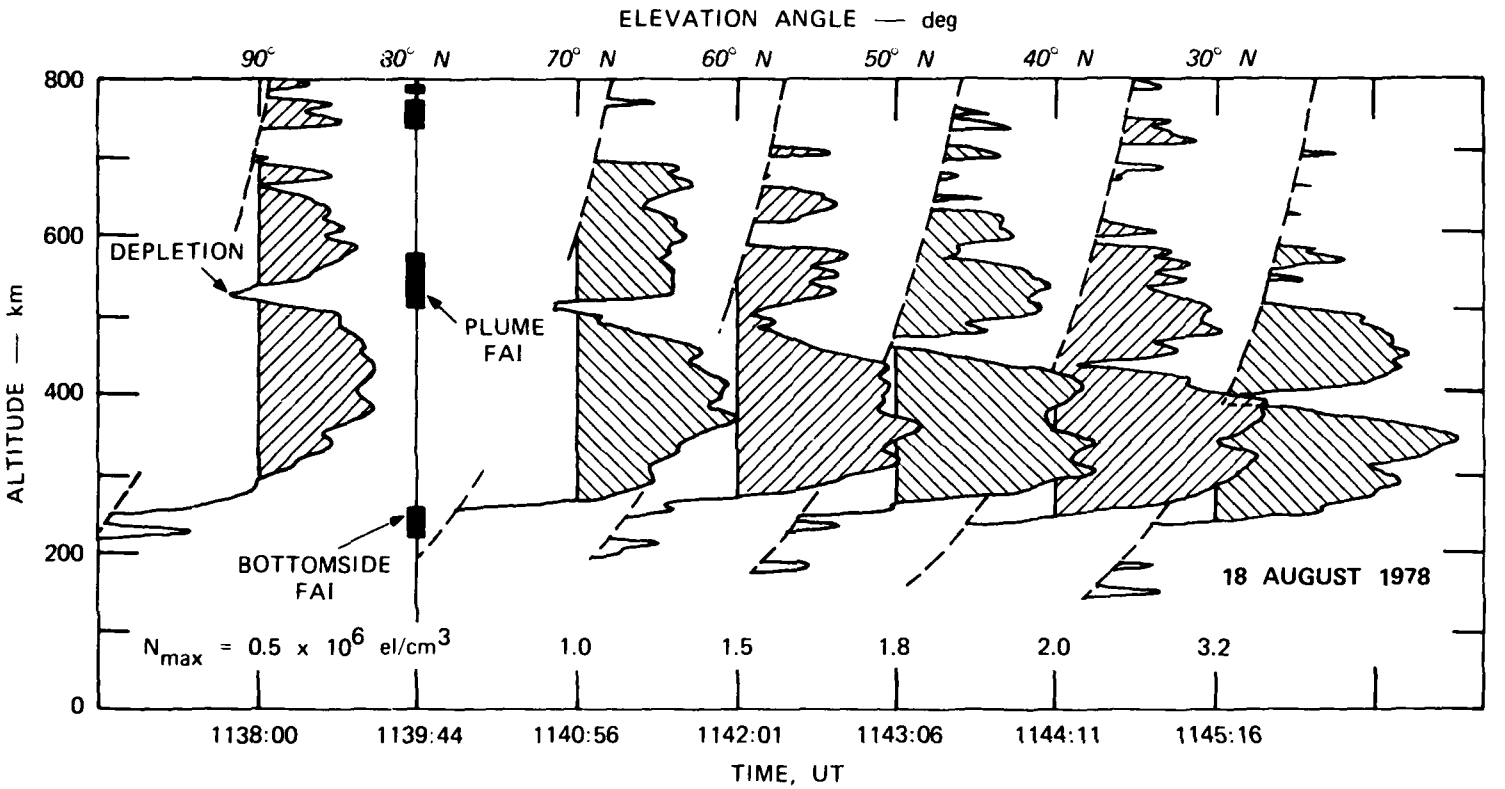

FIGURE 4 ELECTRON DENSITY PROFILES OBTAINED FROM THE NORTH HALF OF THE ELEVATION SCAN BY ALTAIR. (The black vertical bars show the locations of backscatter from FAI.)

Another feature included in the profiles, that should be pointed out before describing the electron density distribution in latitude, is the dashed curve that appears in each of the profiles. These curves represent 1/100th the value of the mean noise power, and can be used to determine whether or not structure in the profiles can be attributed to real variations in electron density. As a rule of thumb,

$$\frac{\sigma_N}{N_e} \approx \frac{SNR^{-1}}{\sqrt{n}} \quad \text{(valid for SNR} \leq 1)$$

where σ_N = standard deviation of electron density

N_e = mean value of electron density

SNR = signal-to-noise ratio

n = number of independent data samples

For this data set (if we do not include the weighted range-averaging), $\sqrt{n} \approx 50$ and SNR can be estimated by comparing the electron density values shown in Figures 3 and 4 to their corresponding mean noise power which is given by the dashed curve. The SNR values range from 0.01 where the electron density profile intersects the dashed curve, to 0.35 near the peak electron density values found in some of the profiles in Figure 4. The error, σ_N/N_e, therefore, ranges from 200% down to 7%.

Examining Figure 3 first (i.e., the south half of the latitude scan), we note several features. All of the profiles are reasonably similar between the altitudes of 300 and 500 km. The profiles tend to be structured but generally flat, with no clear indication of an F-layer peak. Peak electron densities (listed below each profile) range from 6×10^5 el/cm^3 to 4.3×10^5 el/cm^3, decreasing with increasing elevation (or latitude). Above 500 km altitude, the two profiles taken at the lowest elevation angles display a sharp cutoff in electron density with increasing altitude. The third profile (60°S elevation) shows an apparent recovery in electron density at 580 km, 50 km above a similarly sharp cutoff, suggesting that the cutoff in electron density seen in the other profiles is really the lower wall of a plasma depletion, or bubble. This primary

depletion, on which we focus our attention in this paper, is not evident in the profile taken at 70°S elevation, but reappears in the profile taken at 80°S elevation. The reality of this plasma depletion can be seen by its persistence throughout the profiles shown in Figure 4. Although the altitude of the plasma depletion decreases with increasing latitude, it is clear that the depletions are all spatially related. (It is shown later in this section that the decrease in depletion altitude with increasing latitude is consistent with magnetic field alignment of the plasma bubble.) The depth of the depletion, in several cases, exceeds an order of magnitude, or 90%.

Examining the profiles in Figure 4, taken to the north of ALTAIR, it is seen that the peak electron density increases with increasing latitude. The increase is quite substantial, a factor of almost 7.5 in going from the profile taken at 80°S elevation to the profile taken at 30°N elevation. This nonuniform distribution of electron density with latitude is called the equatorial anomaly, and is discussed in the following section. Another plasma bubble is seen to be located approximately 100 km above the primary depletion just described. Because this bubble is located at a higher altitude (where the radar is less sensitive) than the primary bubble, we cannot ascertain whether it is as depleted as the primary bubble.

The final feature in the profiles in Figure 4 worth noting is the systematic decrease in profile altitude-extent with increasing latitude. The decrease in altitude extent can be shown to be a real latitudinal variation and not simply a result of a reduction in radar sensitivity with increasing range. If the variation was due to radar sensitivity, the slant range to the "cutoff" in the topside F layer should be nearly constant. By comparing the slant range at 70°N elevation (750 km) to that at 30°N elevation (approximately 1200 km), it is clear that the cutoff altitude and its variation with latitude is real. (Later, we show that the cutoff altitude is nearly aligned along a magnetic field line.)

The only profile not shown in Figure 4 is that taken at 1139:44 UT. At 80°N elevation, the radar beam is within a degree of perpendicularity with the geomagnetic field lines. Consequently, IS signals were masked

by strong backscatter from FAI. Therefore, instead of displaying the strong backscatter profile in this figure, we have marked the altitude distribution of backscatter from FAI by vertical black bars.

As might be expected from previous results [Towle, 1979; Tsunoda, 1979], the enhanced backscatter regions are related to features in the electron density profiles. Backscatter from bottomside FAI is clearly associated with the base of the F layer. There is also backscatter associated with the primary plasma bubble, and is later shown to be associated with a backscatter plume. Only the backscatter from the highest altitudes cannot be clearly associated with a profile feature. Because of its transient nature, however, (i.e., the topside backscatter dissipated in less than 12 minutes), we do not attempt to discuss its implications.

In an earlier paper Tsunoda [1979] argued, using indirect evidence, that plume backscatter was often associated with the upper wall of the plasma bubble. This data set can be used to verify his conclusion, because the plasma bubble location is determined as a function of time. Because both profiles, taken before and after the backscatter measurements, show the plasma depletion to be situated slightly below the altitude of the enhanced plume backscatter, it may be concluded (for this data set) that the plume backscatter was associated with the upper wall of the plasma bubble.

The results extracted from the electron-density profiles shown in Figures 3 and 4 are summarized in Figure 5. In order to easily visualize the alignment of the various features with the geomagnetic field, a contour plot of F-layer electron density was constructed, using the data in Figures 3 and 4. The contour plot, shown in Figure 5, is plotted in coordinates of altitude and magnetic north distance from ALTAIR (a corresponding magnetic dip latitude scale is shown at the top of the figure). The 10^5 el/cm^3 contour is shown only where reasonably reliable estimates of that electron density could be made. As in Figure 4, black bars are used to locate the ranges at which enhanced backscatter from FAI was detected.

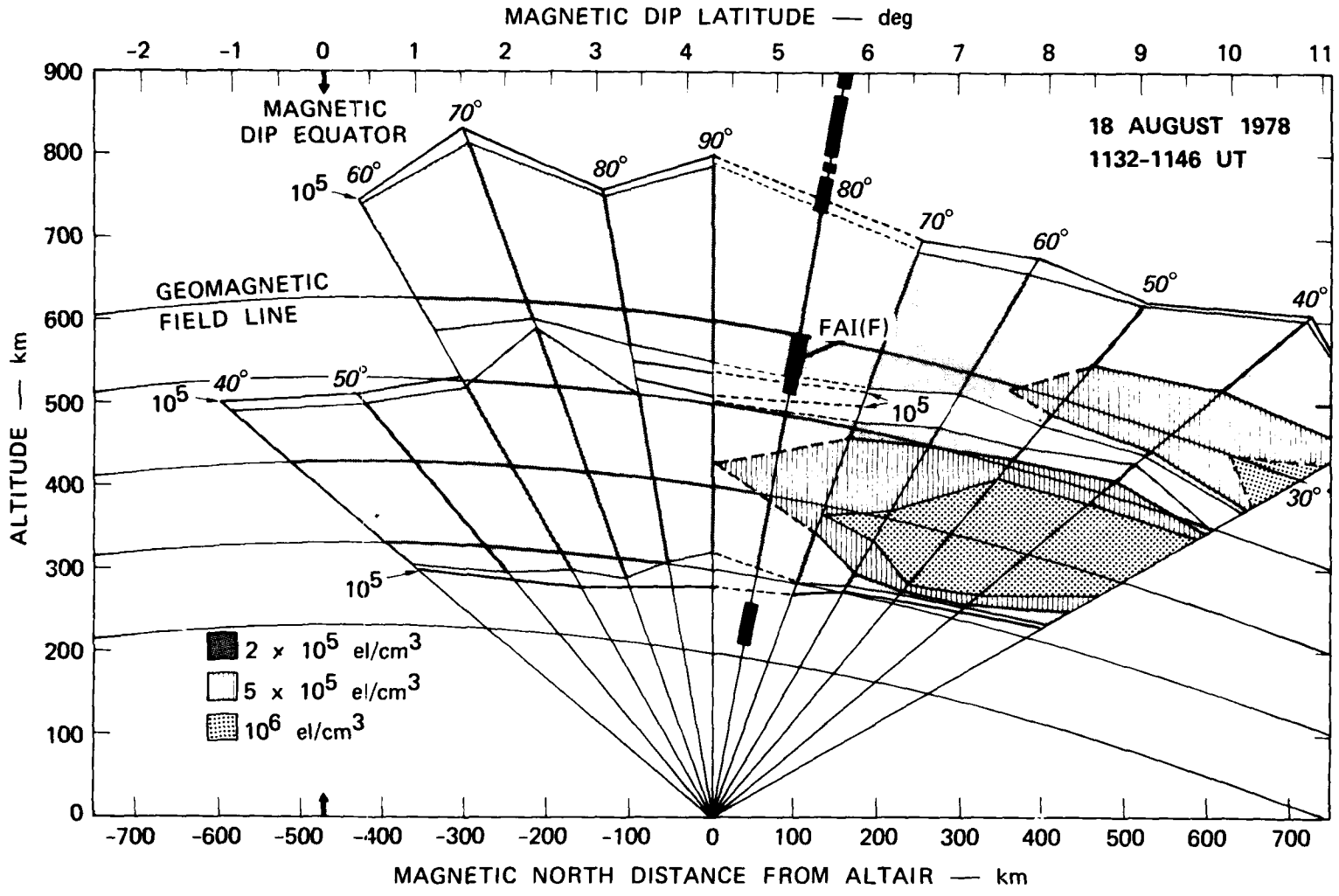

FIGURE 5 CONTOUR MAP SHOWING THE LATITUDINAL DISTRIBUTION OF ELECTRON DENSITY GREATER THAN 2 x 10^5 el/cm^3 (shaded region) AND THE MAGNETIC FIELD ALIGNMENT OF THE PLASMA DEPLETION (gap between shaded regions)

The plasma-depleted region of interest is clearly seen in Figure 5 as a gap separating the two large shaded bands that represent regions containing electron densities greater than 2×10^5 el/cm^3. The curved lines in Figure 5 represent geomagnetic field lines. Comparing these curves to the contours of the gap, we find that the plasma-depleted region is very closely aligned with the magnetic field lines. The depleted region is seen to extend from over the magnetic dip equator to nearly 10° magnetic dip latitude. The topside of the F layer is also field-aligned. And, as discussed above, the enhanced backscatter associated with the plasma bubble, labeled FAI(F), is spatially collocated with the upper wall of the depleted flux tube.

The equatorial anomaly, described above in terms of an increasing peak electron density in the profiles taken with decreasing (north) elevation angles, is clearly seen in the contour plot in Figure 5. Contours of higher electron density are seen to be confined to the north of ALTAIR. The two contour segments, above and below the depleted flux tube, can be interpreted as the lower-latitude portion of the "crest region" in the equatorial anomaly where the electron density accumulates after diffusing down the magnetic field lines from higher altitudes above the magnetic dip equator. In this example, the crest region is bifurcated by the presence of a depleted flux tube. The presence of the equatorial anomaly could result in a plasma bubble whose percentage depletion varies along the magnetic field line (or with latitude).

The excellent alignment of the plasma bubble with magnetic field lines raises the question of whether the vertical bubble velocity was small, in spite of a percentage depletion that often exceeded 90%. We consider whether the observed decrease in depletion altitude with increasing latitude (or time) could be produced by a downward and eastward transport of the F layer, and then estimate the upward bubble velocity.

A comparison of the location of the depletion at 1138:00 UT (90°) with that at 1145:16 UT (30° north), shows the altitude difference to be 135 km. Using the descent rate of the F layer of 13 m/s (or .78 km/min) computed earlier, we estimate that the F layer descended less than 6 km in that time interval. Therefore, if the plasma bubble had a zero upward

velocity relative to the background plasma, the descent rate of the F layer cannot account for the decrease in the altitude of the plasma depletion with increasing latitude.

The effects of eastward bulk-plasma drift can be assessed by examining the east-west spatial distribution of the backscatter plume structure associated with the primary plasma bubble. Such a map, taken immediately after completion of the latitude scan (Figures 3 and 4), is shown in Figure 6. The spatial distribution of backscatter from FAI is shown in the map by contours of constant backscatter strength. Zero dB corresponds to equivalent IS backscatter from an electron density of 10^6 el/cm^3.

Two plumes are seen in the map. The plume of interest is located on the right side of the map, separated from the other plume by a region of no enhanced backscatter. If there were no eastward bulk-plasma drift (and no upward bubble velocity), the plane of the latitude scan would intersect the plume-altitude distribution located in beam-position 13 (measured at 1151:30 UT), shown in Figure 6. If we assume, however, that there was a mean eastward plasma drift of 130 m/s [Woodman, 1972], the latitude-scan measurement (at 1139:44 UT) would have intersected the plume approximately 92 km to the east of beam position 13. Using the slope of the plume in Figure 6, it is estimated that the plume would have been situated 35 km lower in altitude than that shown in beam position 13 at the time of the latitude scan. That is, the plume would have appeared at an altitude of 525 km at 1139:44 UT, 11 minutes 46 seconds before the measurement at beam-position 13 in Figure 6. Instead, it was found in Figure 4 that the plume was centered at 540 km. The 15-km discrepancy can, of course, be attributed to a smaller eastward velocity, or to an upward bubble velocity (relative to the observer). If the discrepancy is caused entirely by upward bubble movement, the velocity would have been 21 m/s. As the slope of the plume is nearly uniform, doubling the eastward drift velocity will double the altitude discrepancy, and in turn, will double the upward bubble velocity to 42 m/s. From this line of reasoning, it can be concluded that upward bubble velocity was probably no more than 40 m/s (and perhaps even zero). And because both eastward bulk-plasma transport and upward bubble

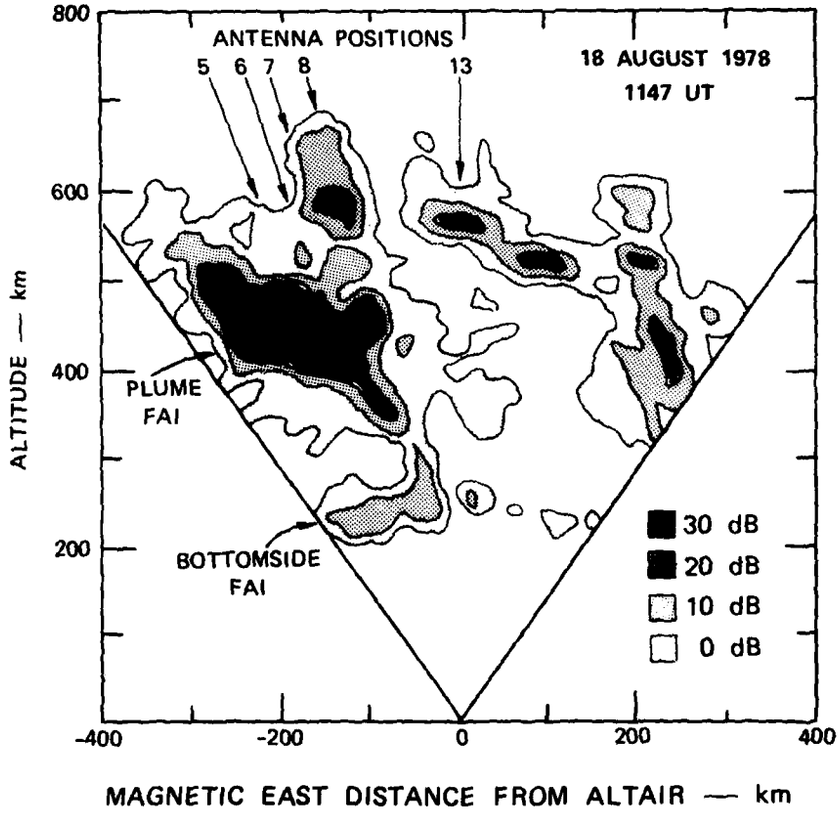

FIGURE 6 CONTOUR MAP SHOWING THE EAST-WEST *vs.* ALTITUDE DISTRIBUTION OF BACKSCATTER FROM FAI. (The plume that corresponds to the major plasma depletion in Figure 4 is shown by the arrow labeled 13.)

velocity result in increased bubble altitude as a function of time, it can also be concluded that most (if not all) of the 135-km decrease in bubble altitude with increasing latitude must be a true spatial variation.

To summarize, the principal results are as follows:

(1) Plasma bubbles are magnetic field aligned and can extend over at least 10° of latitude.

(2) The depth of the primary plasma depletion found in this data set often exceeded an order of magnitude, or 90%.

(3) Plume backscatter in this example was shown to correspond to the upper wall of the plasma bubble.

(4) The upward bubble velocity was no more than 40 m/s, and perhaps as small as zero.

(5) The F layer varied significantly with latitude, up to a factor 7.5 in peak electron density.

IV DISCUSSION

In this report, we have shown direct evidence that plasma bubbles are plasma-depleted regions that extend along geomagnetic flux tubes. The measurements showed that this field alignment extended from over the magnetic dip equator northward to nearly 10° magnetic dip latitude. The depleted region of interest had a vertical dimension transverse to the magnetic field lines of several tens of kilometers. These results are consistent with the theoretical predictions of Farley [1960], and suggests the validity of the assumption that magnetic field lines are electric equipotentials.

The existence of a substantial latitudinal variation in F-layer electron density profile was also shown. In particular, it has been shown that the peak electron density increased by a factor of 7.5 from 3°N magnetic dip latitude to 9°N magnetic dip latitude. The latitudinal variation in F-layer electron density can be explained in terms of an evening enhancement of the equatorial anomaly. That is, the large upward displacement of the F layer that occurred around 0830 UT (see Figure 2) was probably accompanied by plasma diffusion, down geomagnetic field lines, to higher latitudes, resulting in increased electron densities there.

This behavior of the latitudinal distribution of F-layer electron density was theoretically modeled by Anderson [1973] and Huang [1974], using vertical ionospheric velocities measured by the Jicamarca IS radar. Using an upward F-layer velocity of about 40 m/s, Anderson [1973] and Huang [1974] showed that the peak electron density could be made to vary with latitude by as much as a factor of 4. Considering that they used a smaller upward velocity and a larger downward velocity (about 25 m/s) than observed during this event, the results are in good agreement with the theoretical models. Both the upward and downward differences between their model values and those found in this data set can be expected to

enhance electron densities at higher latitudes for a longer time. The persistence of the anomaly to later local times is consistent with the observations in this event, which occurred between 2240 and 2310 local time--somewhat later than the times of peak enhancement of the anomaly predicted by the models.

The substantial latitudinal variation in background plasma density raises an interesting question. What is the expected dynamics of a depleted magnetic flux tube imbedded in such a non-uniform ionosphere? What, furthermore, is the expected latitudinal distribution of plasma-density irregularities within the depleted flux tube? Because plasma bubble evolution and dynamics in the Rayleigh-Taylor instability model is an interchange process, in which a magnetic flux tube maintains its identity and contents, the plasma density within the depleted flux tube--integrated along that field line--should remain constant. If we assume that the plasma density within the flux tube is distributed uniformly along the flux tube, the latitudinal variation in the background plasma density will result in a local percentage depletion of the bubble that is also variable with latitude. Variable percentage depletion would result in variable local bubble velocities and irregularity growth rates [e.g., Ossakow and Chaturvedi, 1978].

The variation of the corresponding transverse polarization electric field (which is proportional to the percentage depletion of the bubble) along the magnetic flux tube implies through the relation curl $\vec{E} = 0$ that a parallel electric field would develop. We would consequently expect field-aligned current-flow in order to keep the current divergence free. It is not yet clear how the presence of parallel electric fields, field-aligned currents, and plasma density distribution (as a function of latitude) will affect the latitudinal distribution of irregularity formation. The implications, however, do not point toward a uniform latitudinal distribution of FAI. An analogous problem of irregularity formation, associated with a barium ion cloud in an inhomogeneous background ionosphere was considered by Goldman et al. [1976].

The non-uniform background F layer clearly indicates that at least flux-tube-integrated values of plasma density and Pedersen conductivity

should be used when comparing observations with predictions by theoretical models. A case in point is the observation in Section III that the plasma bubble rose at a rate of no more than 40 m/s, probably closer to 20 m/s, and possibly as small as zero. For illustration purposes, we assumed that the bubble velocity was no more than 50 m/s. Consider first, the case of a zero ambient electric field. If the predictions of the two-dimensional model presented by Ossakow and Chaturvedi [1979] are now used, one would expect a percentage depletion of no more than 50%, for a bubble located at 400 km altitude. From Figures 4 and 5, it can be noted that the depleted flux tube was at 400 km altitude at 9°N magnetic latitude and that the percentage depletion was closer to 90%. For a 90% depletion, the same theoretical model would predict an upward bubble velocity in excess of 100 m/s. The depleted flux tube extends upward to 550 km altitude over the magnetic dip equator. At 550 km, the two-dimensional model predicts a percentage depletion of less than 10% for an upward bubble velocity of 50 m/s.

On the other hand, Anderson and Haerendel [1979] showed that smaller vertical bubble velocities are obtained by using flux-tube-integrated values. Incorporating the latitudinal distribution of plasma density produced by the post-sunset rise of the F layer, they computed an effective upward bubble velocity over the magnetic dip equator as a function of altitude and local time. The effective bubble velocity (due entirely to the gravitational force term) can be thought of as the limiting upward velocity that a depleted flux tube can attain when the percentage depletion is 100%. For lesser percentage depletions, the upward bubble velocity would be correspondingly smaller. At 1140 UT (2250 LT), the effective bubble velocity was computed to be 75 m/s at 550 km, the bubble velocity over the magnetic dip equator.

Without yet considering the effects of the ambient electric field, we find that the theoretical model using flux-tube-integrated quantities tends to predict results that are closer to our observations. Next, we consider how the inclusion of the ambient electric field will affect this conclusion. A westward electric field that produces the downward movement of the F layer will also contribute a downward component of

bubble velocity. This downward component of bubble velocity will tend to bring the above theoretical estimates in better agreement with our observations. However, the relative contribution of the ambient electric field to the total bubble velocity is smaller at higher altitudes in the case of the two-dimensional model as compared to the flux-tube-integrated model. For example, above 450 km altitude, the bubble velocity in the two-dimensional model is dominated by the gravitational term and the contribution by the ambient electric field is negligible [Ossakow and Chaturvedi, 1978]. For similar altitudes, the bubble velocity in the flux-tube-integrated model is still strongly influenced by the ambient electric field [Anderson and Haerendel, 1979], We find, therefore, that the flux-tube-integrated estimate of vertical bubble velocity is in reasonable agreement with observations; whereas, the velocity estimate from the two-dimensional model using local values is not.

We conclude that care must be taken when interpreting observations quantitatively in terms of predictions by two-dimensional models, using local values of electron density and ion-neutral collision frequency. Models using flux-tube-integrated values appear to predict bubble behavior that is closer to observed bubble behavior. The presence of an evening enhancement in the equatorial anomaly also introduces a local-time dependence of the flux-tube-integrated quantities--which must also be accounted for when predicting bubble dynamics.

..EFERENCES

Anderson, D. N., "A Theoretical Study of the Ionospheric F Region Equatorial Anomaly--II. Results in the American and Asian Sectors," Planet. Space Sci., Vol. 21, p. 421, 1973.

Anderson, D. N. and G. Haerendel, "The Motion of Depleted Plasma Regions in the Equatorial Ionosphere," J. Geophys. Res., Vol. 84, p. 4251, 1979.

Balsley, B. B., G. Haerendel, and R. A. Greenwald, "Equatorial Spread-F: Recent Observations and a New Interpretation," J. Geophys. Res., Vol. 77, p. 5625, 1972.

Dungey, J. W., "Convective Diffusion in the Equatorial F Region," J. Atmos. Terr. Phys., Vol. 9, p. 304, 1956.

Dyson, P. L. and R. F. Benson, "Topside Sounder Observations of Equatorial Bubbles," Geophys. Res. Letts., Vol. 5, p. 795, 1978.

Farley, D. T., "A Theory of Electrostatic Fields in the Ionosphere at Nonpolar Geomagnetic Latitudes," J. Geophys. Res., Vol. 65, p. 869, 1960.

Goldman, S. R., L. Baker, S. L. Ossakow, and A. J. Scannapieco, "Striation Formation Associated with Barium Clouds in an Inhomogeneous Ionosphere," J. Geophys. Res., Vol. 81, p. 5097, 1976.

Haerendel, G., "Theory of Equatorial Spread F," preprint, 1974.

Hanson, W. B. and S. Sanatani, "Large Ni Gradients Below the Equatorial F Peak," J. Geophys. Res., Vol. 78, p. 1167, 1973.

Huang, C. M., "A Certain Behavior of the Ionospheric F2 Region at Low Latitudes," Radio Sci., Vol. 9, p. 519, 1974.

Hudson, M. K. and C. F. Kennel, "Linear Theory of Equatorial Spread F," J. Geophys. Res., Vol. 80, p. 4581, 1975.

Kelley, M. C., G. Haerendel, H. Kappler, A. Valenzuela, B. B. Balsley, D. A. Carter, W. L. Ecklund, C. W. Carlson, B. Hausler, and R. Torbert, "Evidence for a Rayleigh-Taylor Type Instability and Upwelling of Depleted Density Regions During Equatorial Spread-F," Geophys. Res. Letts., Vol. 3, p. 448, 1976.

McClure, J. P., W. B. Hanson, and J. H. Hoffman, "Plasma Bubbles and Irregularities in the Equatorial Ionosphere," J. Geophys. Res., Vol. 82, p. 2650, 1977.

Morse, F. A., B. C. Edgar, H. C. Koons, C. J. Rice, W. H. Heikkila, J. H. Hoffman, B. A. Tinsley, J. D. Winningham, A. B. Christensen, R. F. Woodman, J. Pomalaze, and N. R. Teixeira, "Equion, An Equatorial Ionospheric Irregularity Experiment," J. Geophys. Res., Vol. 82, p. 578, 1977.

Ossakow, S. L. and P. K. Chaturvedi, "Morphological Studies of Rising Equatorial Spread F Bubbles," J. Geophys. Res., Vol. 83, p. 2085, 1978.

Scannapieco, A. J. and S. L. Ossakow, "Nonlinear Equatorial Spread-F," Geophys. Res. Letts., Vol. 3, p. 451, 1976.

Towle, D. M., "VHF and UHF Radar Observations of Equatorial Ionospheric Irregularities and Background Densities," accepted for publication, Radio Science, 1979.

Tsunoda, R. T., "On the Spatial Relationship of 1-Meter Equatorial Spread-F Irregularities and Plasma Bubbles," accepted for publication, J. Geophys. Res., 1979.

Tsunoda, R. T. and D. M. Towle, "On the Spatial Relationship of 1-Meter Equatorial Spread-F Irregularities and Depletions in Total Electron Content," accepted for publication, Geophys. Res. Letts., 1979.

Tsunoda, R. T., M. J. Baron, J. Owen, and D. M. Towle, "ALTAIR: An Incoherent-Scatter Radar for Equatorial Spread-F Studies," in press, Radio Science, 1979.

Weber, E. J., J. Buchau, R. H. Eather, and S. B. Mende, "North-South Aligned Equatorial Airglow Depletions," J. Geophys. Res., Vol. 83, p. 712, 1978.

Woodman, R. F., "East-West Ionospheric Drifts at the Magnetic Equator," Space Res. XII, Vol. 12, p. 969, 1972.

Woodman, R. F. and C. La Hoz, "Radar Observations of F-Region Equatorial Irregularities," J. Geophys. Res., Vol. 81, p. 5447, 1976.

DISTRIBUTION LIST

DEPARTMENT OF DEFENSE

Assistant to the Secretary of Defense
Atomic Energy
ATTN: Executive Assistant

Command & Control Technical Center
ATTN: C-650

Defense Advanced Rsch. Proj. Agency
ATTN: TIO

Defense Communications Agency
ATTN: Code 810, J. Barna
ATTN: Code 101B
ATTN: Code 480, F. Dieter

Defense Communications Engineer Center
ATTN: Code R410, J. McLean
ATTN: Code R820
ATTN: Code R410, R. Craighill

Defense Nuclear Agency
ATTN: STVL
ATTN: RAAE
4 cy ATTN: TITL

Defense Technical Information Center
12 cy ATTN: DD

Field Command
Defense Nuclear Agency
ATTN: FCPR

Field Command
Defense Nuclear Agency
Livermore Division
ATTN: FCPRL

Interservice Nuclear Weapons School
ATTN: TTV

Joint Chiefs of Staff
ATTN: C3S Evaluation Office

Joint Strat. Tgt. Planning Staff
ATTN: JLTW-2

National Security Agency
ATTN: R-52, J. Skillman

NATO School (SHAPE)
ATTN: U.S. Documents Officer

Undersecretary of Defense for Rsch. & Engrg.
ATTN: Strategic & Space Systems (OS)

WWMCCS System Engineering Org.
ATTN: R. Crawford

DEPARTMENT OF THE ARMY

BMD Advanced Technology Center
Department of the Army
ATTN: ATC-T, M. Capps

DEPARTMENT OF THE ARMY (Continued)

Harry Diamond Laboratories
Department of the Army
ATTN: DELHD-I-TL, M. Weiner
ATTN: DELHD-N-P, F. Wimenitz
2 cy ATTN: DELHD-N-P

U.S. Army Comm.-Elec. Engrg. Instal. Agency
ATTN: CCC-EMEO-PED, G. Lane

U.S. Army Foreign Science & Tech. Ctr.
ATTN: DRXST-SD

U.S. Army Satellite Comm. Agency
ATTN: Document Control

U.S. Army TRADOC Systems Analysis Activity
ATTN: ATAA-PL

DEPARTMENT OF THE NAVY

Naval Electronic Systems Command
ATTN: PME 106-4, S. Kearney
ATTN: PME 106-13, T. Griffin
ATTN: Code 501A

Naval Intelligence Support Ctr.
ATTN: NISC-50

Naval Ocean Systems Center
ATTN: Code 532

Naval Research Laboratory
ATTN: Code 4700, T. Coffey
ATTN: Code 7500, B. Wald
ATTN: Code 4780, S. Ossakow
ATTN: Code 7550, J. Davis

Naval Surface Weapons Center
ATTN: Code F31

Strategic Systems Project Office
Department of the Navy
ATTN: NSP-2722, F. Wimberly
ATTN: NSP-2141

DEPARTMENT OF THE AIR FORCE

Air Force Geophysics Laboratory
ATTN: PHP, J. Aarons
ATTN: OPR-1, J. Ulwick
ATTN: PHI, J. Buchau
ATTN: PHP, J. Mullen

Air Force Technical Applications Center
ATTN: TN

Air Force Weapons Laboratory
Air Force Systems Command
ATTN: DYC
ATTN: SUL

Air Force Wright Aeronautical Laboratories
ATTN: A. Johnson

DEPARTMENT OF THE AIR FORCE (Continued)

Ballistic Missile Office
Air Force Systems Command
ATTN: MNNL, S. Kennedy

Foreign Technology Division
Air Force Systems Command
ATTN: NIIS, Library

Headquarters Space Division
Air Force Systems Command
ATTN: SKA, M. Clavin

Rome Air Development Center
Air Force Systems Command
ATTN: TSLD

Strategic Air Command
Department of the Air Force
ATTN: NRT
ATTN: ADWATE, B. Bauer
ATTN: XPFS, B. Stephan

DEPARTMENT OF ENERGY CONTRACTORS

EG&G, Inc.
Los Alamos Division
ATTN: J. Colvin
ATTN: D. Wright

Lawrence Livermore National Laboratory
ATTN: Technical Information Dept.

Los Alamos National Scientific Laboratory
ATTN: MS 664, J. Zinn
ATTN: J. Wolcott
ATTN: R. Jeffries

Sandia National Laboratories
ATTN: D. Dahlgren
ATTN: Org. 1250, W. Brown
ATTN: Org. 4241, T. Wright

OTHER GOVERNMENT AGENCIES

Central Intelligence Agency
ATTN: OSI/PSTD

Institute for Telecommunications Sciences
National Telecommunications & Info. Admin.
ATTN: W. Utlaut

DEPARTMENT OF DEFENSE CONTRACTORS

Aerospace Corp.
ATTN: R. Slaughter
ATTN: I. Garfunkel
ATTN: N. Stockwell

University of Alaska
ATTN: Technical Library

Berkeley Research Associates, Inc.
ATTN: J. Workman

Boeing Co.
ATTN: D. Clauson

DEPARTMENT OF DEFENSE CONTRACTORS (Continued)

Charles Stark Draper Lab., Inc.
ATTN: J. Gilmore
ATTN: D. Cox

Computer Sciences Corp.
ATTN: J. Spoor
ATTN: C. Nail

Cornell University
ATTN: D. Farley, Jr.

Electrospace Systems, Inc.
ATTN: P. Phillips

ESL, Inc.
ATTN: C. Prettie
ATTN: J. Marshall

General Electric Co.
ATTN: F. Reibert

General Electric Company-TEMPO
ATTN: DASIAC
ATTN: W. Knapp

General Research Corp.
ATTN: J. Garbarino
ATTN: J. Ise, Jr.

University of Illinois
ATTN: K. Yeh

Institute for Defense Analyses
ATTN: E. Bauer

International Tel. & Telegraph Corp.
ATTN: Technical Library

JAYCOR
ATTN: S. Goldman

Johns Hopkins University
ATTN: T. Potemra
ATTN: Document Librarian

Kaman Sciences Corp.
ATTN: T. Meagher

Linkabit Corp.
ATTN: I. Jacobs

M.I.T. Lincoln Lab.
ATTN: D. Towle

McDonnell Douglas Corp.
ATTN: Technical Library Services

Mission Research Corp.
ATTN: D. Sappenfield
ATTN: F. Fajen
ATTN: R. Bogusch
ATTN: R. Kilb
ATTN: R. Hendrick

Mitre Corp.
ATTN: B. Adams

DEPARTMENT OF DEFENSE CONTRACTORS (Continued)

Mitre Corp.
ATTN: J. Wheeler
ATTN: W. Foster
ATTN: W. Hall

R & D Associates
ATTN: R. Lelevier
ATTN: C. MacDonald
ATTN: W. Karzas
ATTN: B. Gabbard
ATTN: M. Gantsweg

Rand Corp.
ATTN: E. Bedrozian
ATTN: C. Crain

DEPARTMENT OF DEFENSE CONTRACTORS (Continued)

Science Applications, Inc.
ATTN: L. Linson
ATTN: D. Sachs
ATTN: D. Hamlin

SRI International
ATTN: D. McDaniels
ATTN: C. Rino
ATTN: R. Hake, Jr.
ATTN: R. Leadabrand
ATTN: V. Gonzales
ATTN: W. Chesnut
ATTN: R. Tsundo

Technology International Corp.
ATTN: W. Boquist